analytical chemistry

pubs.acs.org/ac Article

In Situ Measurement of ATP in Single Cells by an Amphiphilic Aptamer-Assisted Electrochemical Nano-Biosensor

Min Jiang, Xiaoxue Xi, Zhen Wu,* Xiuhua Zhang, Shengfu Wang, and Wei Wen*

Cite This: *Anal. Chem.* 2022, 94, 14699−14706 Read Online

ACCESS | Metrics & More | Article Recommendations | Supporting Information

ABSTRACT: In situ and quantitative measurements of adenosine 5′-triphosphate (ATP) in single living cells are highly desired for understanding several sorts of necessary physiological and pathological processes. Due to its small size and high sensitivity, an ultramicroelectrode can be used for single-cell analysis. However, ATP is difficult to detect in single cells because it is nonelectroactive and low in content. Herein, we introduced an electrochemical nano-biosensor based on an amphiphilic aptamer-assisted carbon fiber nanoelectrode (aptCFNE) with high signal-to-noise ratio. The low current (e.g., 60 pA) and the tiny diameter of the tip (ca. 400 nm) of the nanosensor made it noninvasive to living cells. The amphiphilic aptamer has good biocompatibility and can be stably modified to the surface of functionalized electrodes. CFNE, which was modified with ferrocene-labeled aptamer, could quickly and selectively detect ATP content in the nucleus, cytoplasm, and extracellular space of single HeLa cells. The results showed that the ATP contents in the nucleus, cytoplasm, and extracellular space were 568 ± 9, 461 ± 20, and 312 ± 4 μM, respectively. The anticancer drug treatment effects on the cellular level were further recorded, which was of great significance for understanding ATP-related biological processes and drug screenings. This strategy is universally applicable to detect other targets by changing the aptamer sequence, which will greatly improve our understanding of cell heterogeneity and provide a more reliable scientific basis for exploring major diseases at the single-cell level.

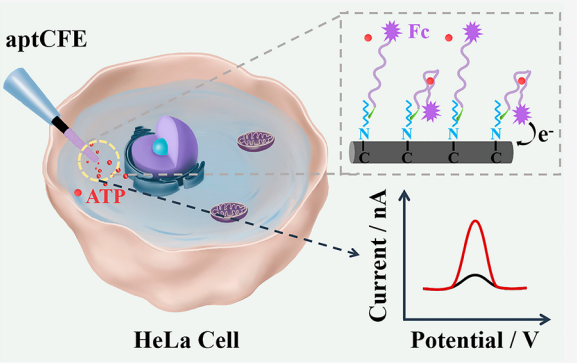

Adenosine 5′-triphosphate (ATP) is the main energy source in living organisms and participates in many biological processes such as biosynthesis and cell metabolism regulation.[1] An abnormal ATP level is usually associated with various kinds of diseases, such as Alzheimer's disease, hypoglycemia, cardiovascular disease, and some malignancies.[2] Some studies suggested that cellular ATP content can be used as an indicator to determine whether some small-molecule drugs and biological agents cause cell damage and proliferation.[3] Moreover, many drugs can cause ATP fluctuation, especially anticancer drugs. Because the population averaging masks differences between individual cells, single-cell analysis (SCA) can elucidate heterogeneity of cells at a deeper level for revealing the nature and law of life activities.[4] SCA can provide accurate information about pathological examination and biomedical therapy and reflect the specific relationship between cell function and chemical components.[5] Therefore, in situ detection of ATP dynamic changes in single cells can provide a more reliable scientific basis for understanding single-cell-related biochemical reactions and drug screening.

Up to now, several strategies including colorimetry, photoelectrochemistry, chemiluminescence, mass spectrometry, surface-enhanced Raman scattering, fluorescence, and electrochemistry have been proposed to detect ATP.[6,7] For example, fluorescent probes for intracellular ATP imaging have been developed, and some can be extended to subcellular organelles.[8] However, current fluorescence methods require the transport of fluorescent probes into the cytoplasm. This is susceptible to issues such as the effect of cytotoxicity on cellular processes, making it impossible to perform long-term and stable analysis.[9] Electrochemical biosensors, owing to their excellent selectivity and good controllability, are used for detecting ATP of cell lysates.[10] Due to the relatively large size of the electrode and slow response, it is difficult to measure intracellular ATP content or monitor its dynamics. Therefore, the development of some highly sensitive and selective nanobiosensors for intracellular ATP detection plays an important role for understanding various biological processes.[11] Because of their low manufacturing cost and adjustable tip size and shape, some electrochemical platforms based on ultra-microelectrodes have emerged as powerful tools for the detection of various biomolecules in single living cells with good temporal

Received: July 17, 2022
Accepted: October 8, 2022
Published: October 17, 2022

https://doi.org/10.1021/acs.analchem.2c03086
Anal. Chem. 2022, 94, 14699−14706

Scheme 1. Illustration of the Amphiphilic Aptamer-Modified Nanosensor for in Situ Detection of ATP in Single Cells[a]

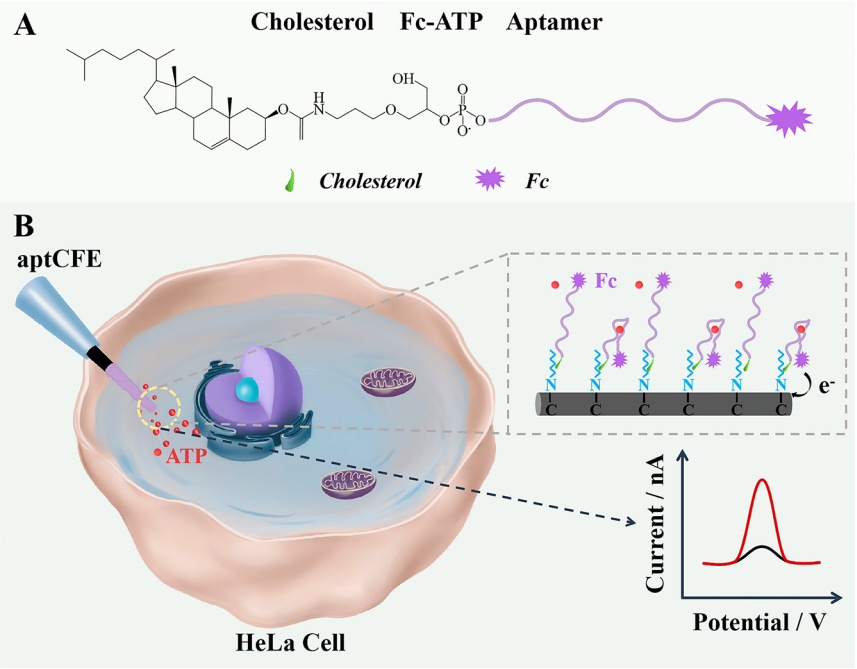

[a](A) Illustration of the amphiphilic aptamer and (B) in situ detection of ATP in the nucleus, cytoplasm, and extracellular space.

and spatial resolution. The enhanced electrochemical signal of the enclosed nanotip provides an opportunity for single-cell electrochemical detection.[12] For example, a carbon fiber nanoelectrode (CFNE) can be fabricated with a conical and tiny tip to enable insertion into a single cell, which shows a high sensitivity and signal-to-noise ratio as well as a fast response. CFNEs were designed as novel nano-biosensors to determine single-cell vesicles, ions, exocytosis, pH, ROS/RNS, and intracellular glucose.[13,14] Significantly, in order to specifically detect the target, CFNEs modified with enzymes, antibodies, single-stranded DNA, aptamers, and other recognition units have been developed for intracellular biomolecular detection.[15]

Among them, aptamers are single-stranded oligonucleotides that specifically bind to target molecules. Because of their simple operation, low immunogenicity, and low cost, aptamers have become a powerful targeting ligand.[16] At present, many aptamer-based electrochemical sensors have been developed.[17] Due to its high hydrophilicity and simple chemical modification, aptamers can be site-specifically ligated with hydrophobic fractions to prepare aptamer−organic amphiphiles (AOAs). At present, a variety of organic components can form AOAs by covalently attaching to aptamers, including the aptamer−lipid amphiphile, aptamer−polymer amphiphile, and aptamer−protein amphiphile.[18,19] AOAs have good biocompatibility and can be stably modified to the surface of functionalized electrodes. For example, the surface of hydrophobic alkylated electrodes can be modified with aptamer−lipid amphiphile owing to the hydrophobic effects between the alkyl chain and lipid. After self-assembly into AOAs, they are widely used in analytical and diagnostic tools. Combining the specific molecular recognition capabilities of AOAs with implantable electrochemical tools enables the creation of highly selective nano-biosensors.[20] In situ biosensors are very suitable for measuring important biomolecules in cells, which provide rich information for exploring cell heterogeneity.[21,22]

In this work, we prepared a simple and sensitive electrochemical nano-biosensor to detect ATP content in three regions of individual HeLa cells. As shown in Scheme 1A, the hydrophobic lipid was labeled on one end of the hydrophilic oligonucleotide to prepare the AOAs. The amphiphilic aptamers were effectively immobilized on the surface of the alkylated CFNEs through the noncovalent interaction of lipid−alkyl chains. Meanwhile, ferrocene was labeled on the other end of the oligonucleotide as an electrochemical signal label. The tip diameters of the CFNEs were controlled to about 400 nm by flame etching, making it noninvasive to detect ATP in living single cells. As shown in Scheme 1B, the conformation of Fc-ATP aptamers was folded in the presence of ATP, resulting in ferrocene being close to the nanoelectrode surface. The oxidation current of ferrocene was increased because electron transfer between ferrocene and the electrode surface was more likely to occur.[23] For intracellular probing, the nano-biosensors could be targeted to specific subcellular regions under the control of 3D micromanipulators, making it possible to quantify ATP in single living cells. The treatment effects of different anticancer drugs (etoposide and oligomycin) were also conducted,[24] demonstrating the potential of the nanotool in dynamically tracking stimulus-induced changes in ATP levels.

EXPERIMENTAL SECTION

Reagents and Materials. Fc-ATP DNA oligonucleotides (5′-chol-TEG-ACCTGGGGGAGTATTGCGGAGGAAGGT-ferrocene-3′) were purified with HPLC and supplied by Sangon Biotech Co. (Shanghai, China). Adenosine 5′-triphosphate (ATP) was purchased from Macklin Biochemical Co. (Shanghai, China). Ferrocenylmethanol (Fc-CH_2OH), guanosine 5′-triphosphate (GTP), cytidine 5′-trophosphate (CTP), uridine 5′-triphosphate (UTP), adenosine 5′-diphosphate (ADP), glucose, etoposide, oligomycin, and C_2H_5OH were supplied by Aladdin Holdings Group Co. (Shanghai,

https://doi.org/10.1021/acs.analchem.2c03086
Anal. Chem. 2022, 94, 14699−14706

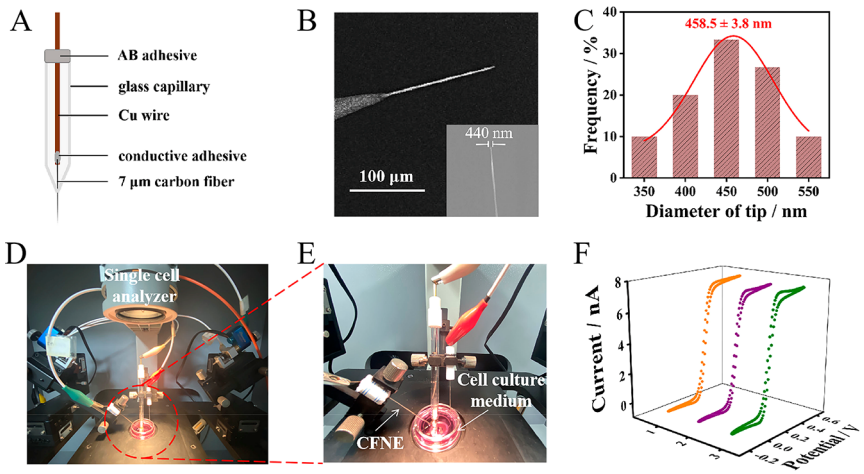

Figure 1. (A) Schematic illustration of the as-prepared CFNE. (B) Scanning electron microscopic image of the tip for the as-prepared CFNE. Inset: the corresponding tip view. (C) Diameter distribution of the tip carbon fiber of CFNE. (D) Partial photograph of a single-cell analyzer. (E) Enlarged photograph showing the holder for fixing and moving the nanoelectrode and three electrode system for electrochemical detection. (F) Typical CVs obtained at bare CFNE in PBS (pH 7.4) containing 2 mM Fc-CH_2OH. Scan rate, 50 mV s^{-1}.

China). Hexylamine (HexA) and lithium perchlorate ($LiClO_4$) were supplied by Sigma-Aldrich. Calcein-AM was purchased from Yeasen (Shanghai, China). Propidium iodide (PI) was purchased from Biosharp (Anhui, China). All aqueous solutions are prepared with deionized water (18.25 MΩ cm).

Apparatus. Electrochemical measurements were carried out with a computer-controlled electrochemical analyzer (CHI 660E, Shanghai, China). FE-SEM (JSM7100F, Jeol) and a microscope (Rayme Biotechnology Co., Jiangsu, China) were used to characterize the fabricated nanoelectrodes. A P1000 laser puller (Sutter Instrument Co., Novato, CA) was used for fabrication of the nanoelectrodes. The XPS measurement was carried out on a Thermo ESCALAB 250Xi instrument. Surface wettability was detected by a contact angle measuring analyzer (OCA50, Dataphysics). A single-cell analyzer (Rayme Biotechnology Co., Jiangsu, China) was used for single-cell analysis.

Cell Culture. HeLa cells were cultured in DMEM (Gibco) containing 10% fetal bovine serum (FBS, VivaCell) and 1% antibiotics (Gibco) with 5% CO_2 at 37 °C for 24 h. The cells were incubated with relative low density in the confocal cell culture dish at 37 °C for 24 h before single-cell analysis. Calcein-AM and PI at a final concentration of 3 μg/mL were added to the cell culture medium to stain these cells and to confirm the cell viability. After incubation with cell culture conditions for 30 min, the residual dyes were washed off.

Preparation of the Nanoelectrode. The carbon fiber nanoelectrodes (CFNEs) were fabricated as follows. First, the carbon fibers (7 μm in diameter) were washed with acetone to dissolve the surface resin coating on the carbon and then dried thoroughly at room temperature. A clean glass capillary (i.d. 0.5 mm) was pulled on a microelectrode puller (Sutter Instrument Co.) into two capillaries. The fine tip of each was pulled to 10−20 μm in diameter. A single carbon fiber was chosen and attached to a copper wire with conductive adhesive. The carbon fiber−Cu wire was carefully inserted into the fine end of the glass capillary, and the other end was sealed with AB adhesive. The tip of glass capillary containing a single carbon fiber was then sealed with the flame of an alcohol lamp enabling a length of 150 μm as well as a diameter of 400 nm under the microscope. The prepared CFNEs were ultrasonically washed with deionized water, ethanol, and deionized water sequentially, each for 3−5 min.

Fabrication of the Nanosensor. Prior to modification, the obtained carbon fiber nanoelectrodes (CFNEs) were electroactivated in 1 M NaOH with 1.5 V-controlled amperometry for 80 s. Then, CV was carried out for the CFNEs at a scanning rate of 0.05 V s^{-1} in the potential range 0−1.0 V until a stable CV was obtained. CFNEs modified with hexylamine (HexA/CFNEs) were obtained by 5 cyclic voltammetry cycles in 5 mM hexylamine ethanol solution with 0.1 M $LiClO_4$ under the cyclic potential from −0.2 to +1.6 V at a scan rate of 10 mV s^{-1}. All DNA oligonucleotides were dissolved in DEPC water at a concentration of 10 μM. DNA stock solution was stored at −20 °C. Before immobilization, DNA solution was allowed to heat to 95 °C for 3 min, followed by rapidly cooling it to room temperature. HexA/CFNEs modified with DNA aptamer (aptCFNEs) were prepared by immersion in 1 μM DNA oligonucleotide solution for 12 h at room temperature, and in 0.5 mM cholesterol-TEG5000 for 1 h as a blocking treatment, respectively. In each step, the electrodes were rinsed with deionized water. The as-modified nanoelectrodes were used as the nanosensors for detection.

Electrochemical Measurement of ATP in Solution or in Cells. A nanosensor, platinum wire, and Ag/AgCl were used as the working electrode, counter electrode, and reference electrode, respectively. The as-prepared nanosensors were immersed in the fixed solution or in cells within 5 min for reaction at room temperature. After the reaction, an electrochemical measurement was conducted in solution or cells using DPV in the potential range 0.1−0.5 V. The background electrochemical signals of the nanosensors were measured and recorded as I_0 in the absence of ATP. In the presence of ATP, the current response was recorded as I_n. In this work, we achieved ATP quantification by $\Delta I/I_0$ (increasing peak current $\Delta I = I_n - I_0$) and varying ATP concentrations at the potential of 0.32 V to minimize the electrode variation. Assisted with a single-cell analyzer (Rayme Biotechnology Co.), the aptCFNEs were inserted into the nucleus, cytoplasm, and extracellular space (near the cell membrane) in single HeLa cells for electrochemical detection. The potential of the nano-biosensor

https://doi.org/10.1021/acs.analchem.2c03086
Anal. Chem. 2022, 94, 14699−14706

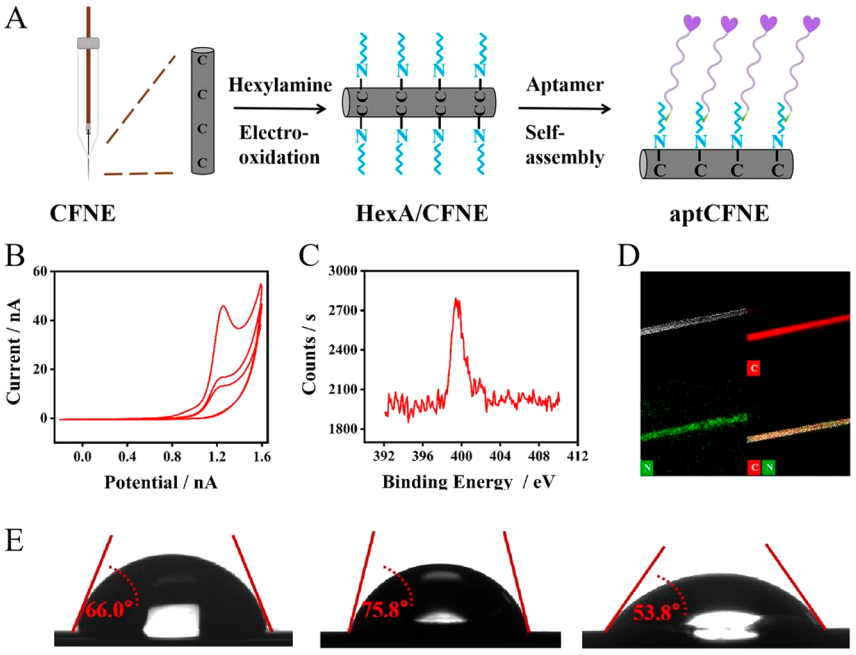

Figure 2. (A) Schematic illustration of cholesterol Fc-ATP aptamer-modified CFNE. (B) CVs of CFNE upon scanning in 0.1 M $LiClO_4$ ethanol solution with 5 mM HexA. Scan rate, 10 mV s^{-1}. (C) N (1s) binding energy on the HexA/CFNE surface. (D) Elemental (C, N) mapping images of HexA/CFNE. (E) Contact angle measurements of GCE, HexA/GCE, and aptGCE.

for probing drug effects was exemplified by etoposide-provoked ATP inducement and oligomycin-inhibited ATP depletion. HeLa cells were incubated in 100 μM etoposide for 20 min or 3 μg/mL oligomycin for 3 h, and subcellular positions of the nucleus, cytoplasm, and extracellular space were then probed. An electrochemical measurement was directly conducted in cells by using DPV. The relevant parameters of DPV were as follows: initial potential (0.1 V), final potential (0.5 V), incremental potential (0.004 V), amplitude (0.05 V), pulse width (0.05 s), sampling width (0.0167 s), pulse period (0.5 s), quiet time (2 s), and sensitivity (e^{-10} A/V).

RESULTS AND DISCUSSION

Preparation of Amphiphilic Aptamer-Modified CFNE.

Preparation of the CFNE was performed as reported in Figure S1, and the final morphology of the CFNE is shown in Figure 1A. A flame etching method was proposed for sealing and controlling the tip of CFNE to be conical and tiny for single-cell analysis. The tip morphology of the nanoelectrode was characterized by scanning electron microscopy (SEM) (Figure 1B and Figure S2A) and a microscope (Figure S2B). As shown, the CFNE possessed a near-conical nanotip with a diameter of about 440 nm. The average diameter and length of CFNE were about 458.5 ± 3.8 nm and 191.6 ± 0.7 μm, respectively, by randomly measuring 50 nanoelectrodes (Figure 1C and Figure S2D). Figure 1D,E shows the photographs of experimental equipment for the electrochemical measurement of single living cells. The ultra-micro-scale tip enabled the nanoelectrode to maintain cell viability after insertion into single cells. The as-obtained CFNE was further characterized by CV scanning in 2 mM Fc-CH_2OH. The typical CV curves were obtained with little difference between nanoelectrodes, which indicated successful fabrication of the CFNE and met the requirement of parallel experiments (Figure 1F).

Primary alkylamine can be modified onto glass carbon electrode (GCE) surfaces by electrochemical oxidation, and the alkyl chains were outward to form a hydrophobic monolayer interface.[25] The strategy can be generalized to modify the surface of CFNE because of the similar chemical nature between it and GCE.[26] To obtain the alkyl chain-modified CFNE, the as-prepared CFNE was functionalized by immersing it into hexylamine (HexA) ethanol solution with $LiClO_4$ under 5 consecutive CV scans (Figure 2B). Specifically, HexA was chosen to construct a hydrophobic surface as well as a minimum distance for effective electron transfer. As shown, an irreversible and definite oxidation peak occurred at a potential of 1.40 V. During the 5 cycles, the peak current was gradually decreasing, and the peak voltage moved to a positive value until finally disappearing, which was mainly due to the amino group of hexylamine being successfully oxidized to the corresponding amino cation radical.[27] Furthermore, the XPS data showed that the N (1s) binding energy on the HexA/CFNE surface was around 399.5 eV, which was consistent with the formation of a carbon−nitrogen bond between the amino cation radical and an aromatic moiety of the CFNE surface (Figure 2C).[28] In contrast, the N (1s) binding energy of aliphatic amines is near 398.0 eV.[29] Figure 2D shows the elemental mapping images of C and N elements, proving their uniform distribution on the surface of CFNE. These results demonstrated that HexA was successfully modified to the CFNE surface (HexA/CFNE) via a carbon−nitrogen bond.

The surface of HexA/CFNE was further modified with aptamer−organic amphiphiles (AOAs) to fabricate the nanosensor (aptCFNE). The hydrophobic lipid was labeled on one end of the hydrophilic oligonucleotide to prepare the AOAs. Importantly, AOAs have good biocompatibility and selectivity for ATP at the subcellular level and can be stably modified to the surface of functionalized electrodes. Herein, the surface of the alkylated CFNE was effectively modified with cholesterol-Fc-ATP aptamer through the noncovalent interaction of lipid−

https://doi.org/10.1021/acs.analchem.2c03086
Anal. Chem. 2022, 94, 14699−14706

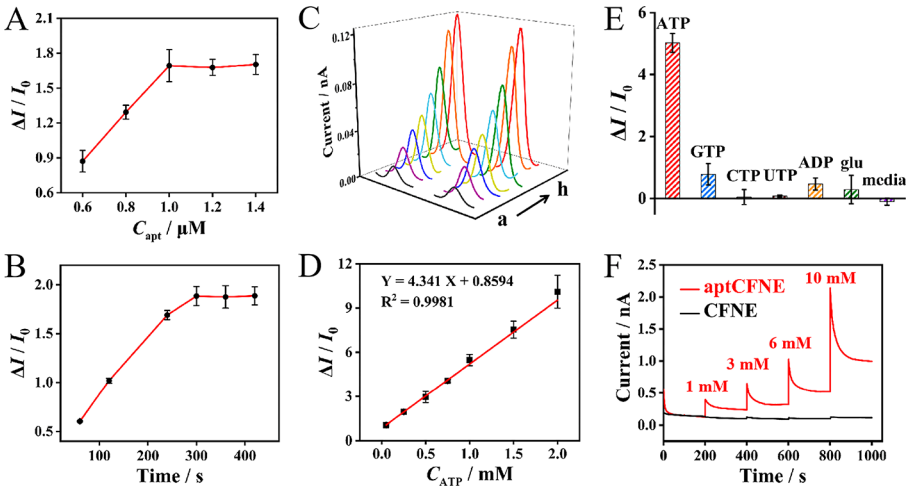

Figure 3. Effect of (A) aptamer concentration and (B) nanoelectrode incubation time on $\Delta I/I_0$ (increasing peak current $\Delta I = I_n - I_0$) with 0.25 mM ATP. (C) Two sets of DPV responses of aptCFNEs in 10 mM PBS (pH 7.4) containing different ATP concentrations, ranging from 0, 0.05, 0.25, 0.50, 0.75, 1.0, 1.5, to 2.0 mM (a–h). (D) Linear relationship between $\Delta I/I_0$ and ATP concentrations. (E) Selectivity of aptCFNEs to 1.0 mM ATP, 5.0 mM ATP analogues (GTP, CTP, UTP, and ADP), 25 mM glucose, and cell culture medium. (F) Amperometric current responses of aptCFNE and CFNE to the continuous addition of ATP (1, 3, 6, and 10 mM) in PBS (pH 7.4).

alkyl chains. Notably, modifying negatively charged oligonucleotides on the electrode surface could make it more hydrophilic, which could be investigated by a contact angle measuring analyzer. Herein, GCE was used to carry out surface wettability. Figure 2E shows that the contact angles of bare GCE and HexA/GCE were determined to be 66° and 75.8°. The increase of contact angles was mainly due to the presence of 6-carbon alkyl chains with moderate hydrophobicity on the electrode surface after electrooxidation. Furthermore, the contact angle of aptGCE was significantly reduced by 22°, indicating that the electrode surface was highly hydrophilic, which suggested the successful immobilization of negative oligonucleotide. These results demonstrated the successful fabrication of the nano-biosensor with a tip diameter of about 400 nm, which is expected to be used to detect intracellular ATP.

Optimization and Feasibility of the Nano-Biosensor. For better intracellular application performance, the reaction conditions of the system were optimized, including aptamer concentration and ATP reaction time. The aptamer concentration, which was used to modify the nanoelectrode, was initially studied. The $\Delta I/I_0$ elevated with aptamer concentration ranging from 0.6 to 1 μM, and after that, it began to level off (Figure 3A). 1 μM was chosen as the optimal aptamer concentration. After fixing the aptamer concentration, the effect of ATP reaction time on the current signal was further studied. As shown in Figure 3B, aptCFNE could respond to ATP within 1 min. With the increase of ATP reaction time, $\Delta I/I_0$ increased and then reached a plateau at 5 min, which was chosen as the optimal reaction time between aptamer and ATP. Under the optimized conditions, every 20 aptCFNEs were used to measure the same concentration of ATP. As shown in Figure S3A, the small error bars of the histograms indicated that variations between different electrodes were small and met the requirements of parallel experiments. Six sets of control experiments were performed to characterize and validate the feasibility of nano-biosensors by DPV (Figure S3B). As shown, there was a large current response of aptCFNE only in the presence of ATP, which indicated that the signal change was produced by the interaction between cholesterol-Fc-ATP aptamer and ATP. To verify the stability of cholesterol-alkyl chains, aptCFNEs were stored in a refrigerator at 4 °C for 7 days. The current of aptCFNEs retained 92% of its initial current intensity (Figure S4). Contrarily, no electrochemical signals were detected by bare CFNEs and HexA/CFNEs, indicating the good storage and reaction stability of the aptCFNEs.

Furthermore, the DPV response of aptCFNE toward ATP concentration in aqueous solution was investigated (Figure 3C). These two sets of curves were collected from multiple aptCFNEs, and the small differences between nanoelectrodes satisfied the requirement of parallel experiments. As shown in curve a, a relatively small ferrocene-oxidation peak was observed at 0.32 V in the absence of ATP. The low background signal (I_0) facilitated highly sensitive detection of ATP because of the tiny tip of CFNE. The fabricated nanosensor was further used to detect solutions with ATP concentrations ranging from 0.05 to 2.0 mM, which matched the concentration of intracellular ATP.[30] As shown in curves b–h, the peak current (I_n) gradually increased with ATP concentration. The selective recognition between the aptamer and ATP could bring ferrocene close to the surface of the nanoelectrode, and more aptamer segments could be folded with higher ATP concentration, resulting in the increase of electrochemical signal. Figure 3D showed a good linearity between $\Delta I/I_0$ and ATP concentration, ensuring the excellent sensitivity of the nano-biosensor for ATP sensing. The linear regression equation was $\Delta I/I_0 = 4.341C_{ATP}$ (mM) + 0.8594 (R = 0.9981), and the detection limit was 3.4 μM (S/N = 3). The selectivity of the aptCFNE was further studied by reacting with ATP analogues (e.g., GTP, CTP, UTP, and ADP), glucose (glu), and cell culture media, respectively. As shown in Figure 3E, only ATP could generate a significant DPV signal. This indicated that the nanosensor exhibited good selectivity and sensitivity, which enabled it to recognize ATP in complex systems. Moreover, the amperometric current responses were observed, which were obtained with aptCFNE and CFNE toward the successive addition of ATP (1, 3, 6, and 10 mM) into PBS (pH 7.4) (Figure 3F). The current response of aptCFNE continuously increased with ATP concentration (red

https://doi.org/10.1021/acs.analchem.2c03086
Anal. Chem. 2022, 94, 14699–14706

curve), while that of CFNE did not change much (black curve), indicating that the nanosensor responded quickly to ATP. All of the above experimental results verified the reliability and feasibility of the nano-biosensor, which is expected to detect ATP at the subcellular level.

In Situ Measurement of Intracellular ATP. In situ detection of ATP at the subcellular level is significant for analyzing disease-specific gene expression and cellular heterogeneity. Assisted by a 3D micromanipulator, microscopy, and electrochemical workstation of the single-cell analyzer, this nanosensor was precisely moved to individual HeLa cells at the subcellular level, and electrochemical assays were carried out with good spatial resolution (Figure 1D,E). After placing the cell culture dish on the micromanipulator, the nanoelectrode could be positioned at the subcellular level by adjusting the $X/Y/Z$ axis with a remote control.[31,32] As shown in Figure 4A, the aptCFNE could easily penetrate into the nucleus, cytoplasm, and extracellular space (near the membrane) due to its conical and tiny tip. When using nanoelectrodes for intracellular studies, it was critical to ensure that the target cells were still alive after the insertion and electrochemical detection. In the experiment, fluorescence dyes (Calcein-AM and PI) were applied to stain the HeLa cells and study its viability. Fluorescence image of cells remained unchanged after insertion and removal of aptCFNE from individual cells, confirming that individual cells remained viable (Figure 4B). More specifically, Figure S5 showed that the cell morphology did not change significantly after the nanosensor was inserted into cytoplasm for 20 min and into the nucleus for 10 min. This further demonstrated that cells remained active when using the nanosensor for detection at the subcellular level. The cell morphology was further observed after electrochemical detection and removal of the aptCFNE (Figure S6). As shown, the morphology of the target cell remained, demonstrating that the electrochemical testing process had little effect on cell viability. Together, these results demonstrated the feasibility of using the aptCFNE to probe intracellular ATP while keeping cells viable.

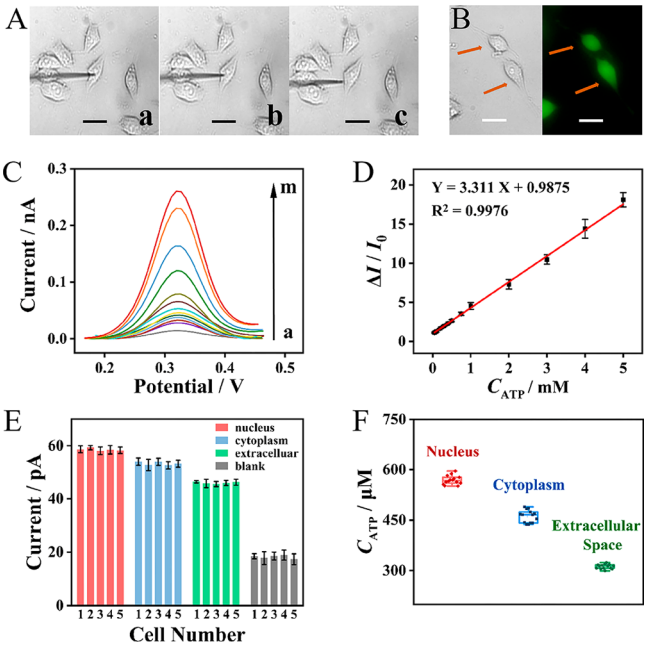

Figure 4. (A) Bright-field microscopy images of controlling the aptCFNE into the (a) nucleus, (b) cytoplasm, and (c) extracellular space. (B) Representative bright-field and fluorescence images of HeLa cells stained with Calcein-AM. Scale bar: 20 μm. (C) DPV responses of aptCFNEs in cell culture media containing different ATP concentrations ranging from 0 to 0.05, 0.1, 0.2, 0.3, 0.4, 0.5, 0.75, 1, 2, 3, 4, and 5 mM (a−m). (D) Corresponding calibration plot between $\Delta I/I_0$ and ATP concentrations. (E) Histograms of the current response of aptCFNEs after being inserted into different regions. (F) Box graph of the calculated ATP concentrations of 15 individual HeLa cells.

The nanosensor was incubated in cell culture media within ATP for 5 min, and a DPV test was carried out. As shown in Figure S7, there was no electrochemical reaction on bare CFNE in cell media. As shown in Figure 4C, the signal responses increased gradually as ATP concentration increased from 0.05 to 5 mM, spanning 2 orders of magnitude. In single cells, the content of ATP is low and above the linear range can satisfy experimental requirements. Figure 4D shows a good linearity between $\Delta I/I_0$ and ATP concentration, ensuring that the aptCFNE could detect ATP with high sensitivity under complex physiological conditions. The corresponding linear regression equation was $\Delta I/I_0$ (nA) = $3.311C_{ATP}$ (mM) + 0.9875 (R = 0.9976), and the detection limit was 4.5 μM (S/N = 3).

Due to its high selectivity and sensitivity, the as-prepared nano-biosensor was then used to detect ATP in individual living cells by DPV. Three different subcellular regions, i.e., the nucleus, cytoplasm, and extracellular space (near the cytomembrane), were spatially selected. As shown in Figure S8, there was no specific peak current of bare CFNE when inserted into cells. Other substances did not interfere with the peak current detected by DPV when intracellular ATP was electrochemically detected, implying that the response current was due to ferrocene on the nanoelectrode surface and intracellular ATP. Considering cell heterogeneity, the current signals for ATP were the statistical results of 15 single cells.[33,34] As shown in Figure 4E, the current histogram exhibited a relative difference between three subcellular regions of HeLa cells. The background electrochemical signals were noticeable lower than the peak current inserted into the specific regions of the single cells. The signals of the nucleus were higher than those of the cytoplasm (mean ± SD: 58.5 ± 0.5 pA vs 53.2 ± 0.6 pA, P < 0.01), probably because ribosomes on the endoplasmic reticulum (present near the nucleus) were involved in protein synthesis, which required a lot of energy.[35] The signals of the extracellular space were lower than those in the cytoplasm (mean ± SD: 45.9 ± 0.3 pA vs 53.2 ± 0.6 pA, P < 0.01), which might be due to the existence of mitochondria in the cytoplasm and specific channels in the cell membrane that participate in intracellular ATP transport under certain conditions. Owing to the cell heterogeneity, the peak current varied slightly between cells in the same regions with an RSD of 0.7−1.2%. According to the as-obtained calibration curve (Figure 4D), the ATP concentration was then estimated to be 568 ± 9, 461 ± 20, and 312 ± 4 μM in the nucleus, cytoplasm, and extracellular space, respectively (Figure 4F). To our knowledge, the results were similar to those reported previously.[36] The results demonstrated that the nano-biosensor can be used as a high-selectivity and high-sensitivity nanotool for in situ detection of ATP in single cells.

Dynamic Assessment of ATP under Drug Effects at the Subcellular Level. The change of intracellular ATP is closely related to many diseases and pathology. Since

https://doi.org/10.1021/acs.analchem.2c03086
Anal. Chem. 2022, 94, 14699−14706

deficiency or excess of important endogenous species has severe biochemical consequences, it is important to study the effects of external drug stimuli on cellular status. Considering the important role of ATP in cell biology, the as-prepared electrochemical nano-biosensor was used to conduct experiments of ATP increment and decrement by anticancer drugs (etoposide and oligomycin).[37] The aptCFNE was inserted into different regions with an incubation time of 5 min, and electrochemical signals were recorded. As shown in Figure 5A,

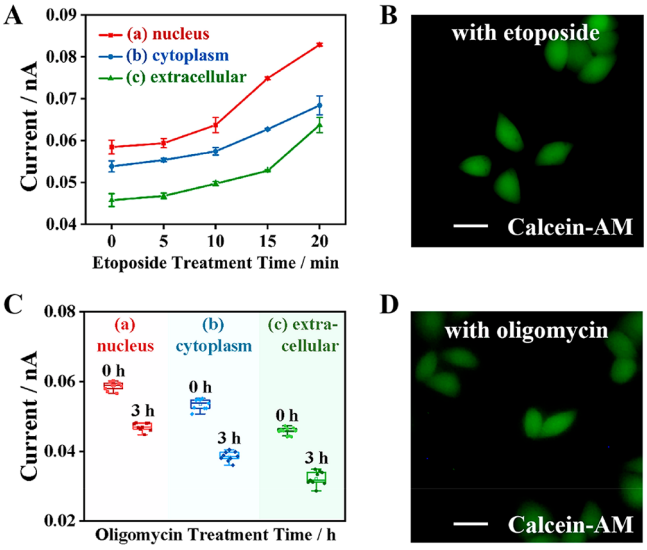

Figure 5. Peak currents of 9 individual HeLa cells after treatment with (A) 100 μM etoposide for 20 min and (C) 3 μg/mL oligomycin for 3 h at subcellular positions of the (a) nucleus, (b) cytoplasm, and (c) extracellular space. (B, D) Fluorescence images of living HeLa cells stained with Calcein-AM after treatment with etoposide and oligomycin. Scale bar: 20 μm.

the current signals of three regions showed an increasing trend during a 20 min etoposide treatment. For example, the average peak current of the nucleus barely changed within the first 5 min and then increased stepwise from 0.059 nA at 5 min to 0.064 nA at 10 min, to 0.075 nA at 15 min, and finally to 0.083 nA at 20 min. The calibration curve in Figure 4D was then used to calculate ATP concentration changes in different regions after treating with etoposide (Figure S9). The Calcein-AM experiment showed that there was no significant effect on cell viability after drug treatment as well as subsequent detection by aptCFNE (Figure 5B). Overall, etoposide could increase intracellular ATP content. It was reported that the mechanism of the etoposide included inhibition of nucleoside transfer and synthesis of DNA, RNA, and protein, and it could promote the synthesis of ATP.[38]

On the other hand, the function of oligomycin is to reduce ATP synthesis by inhibiting oxidative phosphorylation.[39] The temporal change of the intracellular ATP level was followed during a 3 h oligomycin treatment. As shown in Figure 5C, the peak current in the nucleus, cytoplasm, and extracellular space decreased from 0.059 to 0.047 nA, from 0.053 to 0.038 nA, and from 0.046 to 0.032 nA, respectively. Figure 5D shows the cell viability during the experiment, which was demonstrated by staining with Calcein-AM. The ATP concentrations were then calculated according to the calibration curve in Figure 4D after treating with oligomycin (Figure S10). Together, these results unequivocally demonstrated the capability of the nanosensor for probing intracellular ATP fluctuations at the subcellular level following drug stimulation, which was of great significance for understanding single-cell-related physiological processes and drug screening.

CONCLUSION

In conclusion, a novel and universal nano-biosensor (aptCFNE) was constructed by combining amphiphilic aptamer and a carbon fiber nanoelectrode for in situ single-cell analysis. The fabrication process of the nanosensor and operation process of detection were relatively simple. Importantly, the aptCFNE with a tip diameter of about 400 nm could quickly respond to ATP within 5 min, which ensured the detection of intracellular ATP under the premise of maintaining cell viability. Assisted with the single-cell analyzer, the aptCFNE with high sensitivity and selectivity could be localized to different regions of individual HeLa cells (e.g., nucleus, cytoplasm, and extracellular space) for the detection of intracellular ATP. For example, the concentration of ATP in the nucleus was detected to be 568 ± 9 μM, which was higher than that in the cytoplasm (461 ± 20 μM). The dynamic assessment of ATP under anticancer drug effects at the subcellular level was further carried out, which will be of great significance for understanding the single-cell-related physiological process and drug screening.

ASSOCIATED CONTENT

Supporting Information

The Supporting Information is available free of charge at https://pubs.acs.org/doi/10.1021/acs.analchem.2c03086.

Preparation diagram of CFNE, characterization of CFNE, study of the feasibility of the nano-biosensor in detecting ATP, study of the stability of noncovalent interaction between cholesterol-alkyl chains, representative bright-field images of the nanosensor inserted into the cytoplasm or nucleus for different times, representative bright-field and fluorescent images of the nanosensor after the electrochemical testing process, DPV responses of a bare nanoelectrode and nanosensor in cell culture media, DPV responses of electrodes inserted into different regions of cells under different conditions, and dynamic evaluation of ATP content in different regions of a single cell treated with etoposide and oligomycin (PDF)

AUTHOR INFORMATION

Corresponding Authors

Zhen Wu − *Collaborative Innovation Center for Advanced Organic Chemical Materials Coconstructed By the Province and Ministry, Ministry of Education Key Laboratory for the Synthesis and Application of Organic Functional Molecules, College of Chemistry and Chemical Engineering, Hubei University, Wuhan 430062, P. R. China*; Email: wuzhen@hubu.edu.cn

Wei Wen − *Collaborative Innovation Center for Advanced Organic Chemical Materials Coconstructed By the Province and Ministry, Ministry of Education Key Laboratory for the Synthesis and Application of Organic Functional Molecules, College of Chemistry and Chemical Engineering, Hubei University, Wuhan 430062, P. R. China*; orcid.org/0000-0001-6138-7470; Email: wenwei@hubu.edu.cn

https://doi.org/10.1021/acs.analchem.2c03086
Anal. Chem. 2022, 94, 14699−14706

Authors

Min Jiang − *Collaborative Innovation Center for Advanced Organic Chemical Materials Coconstructed By the Province and Ministry, Ministry of Education Key Laboratory for the Synthesis and Application of Organic Functional Molecules, College of Chemistry and Chemical Engineering, Hubei University, Wuhan 430062, P. R. China*

Xiaoxue Xi − *Collaborative Innovation Center for Advanced Organic Chemical Materials Coconstructed By the Province and Ministry, Ministry of Education Key Laboratory for the Synthesis and Application of Organic Functional Molecules, College of Chemistry and Chemical Engineering, Hubei University, Wuhan 430062, P. R. China*

Xiuhua Zhang − *Collaborative Innovation Center for Advanced Organic Chemical Materials Coconstructed By the Province and Ministry, Ministry of Education Key Laboratory for the Synthesis and Application of Organic Functional Molecules, College of Chemistry and Chemical Engineering, Hubei University, Wuhan 430062, P. R. China;* orcid.org/0000-0003-3586-9921

Shengfu Wang − *Collaborative Innovation Center for Advanced Organic Chemical Materials Coconstructed By the Province and Ministry, Ministry of Education Key Laboratory for the Synthesis and Application of Organic Functional Molecules, College of Chemistry and Chemical Engineering, Hubei University, Wuhan 430062, P. R. China;* orcid.org/0000-0001-7175-4908

Complete contact information is available at: https://pubs.acs.org/10.1021/acs.analchem.2c03086

Notes

The authors declare no competing financial interest.

■ ACKNOWLEDGMENTS

This work was supported by the National Natural Science Foundation of China (22076041, 22274037, and 21904032).

■ REFERENCES

(1) Wang, Y. W.; Zhang, D.; Zeng, Y.; Ye, X. Y.; Sun, Y.; Zhou, W. M.; Qi, P. *Sens. Actuators B Chem.* **2021**, *334*, 129609.

(2) Zhou, Y. Z.; Zou, L. N.; Li, G. P.; Shi, T. H.; Yu, S. Y.; Wang, F.; Liu, X. Q. *Anal. Chem.* **2021**, *93*, 13960−13966.

(3) Bohrmann, L.; Burghardt, T.; Haynes, C.; Saatchi, K. *Theranostics.* **2022**, *12*, 4010−4050.

(4) Norregaard, K.; Metzler, R.; Ritter, C. M.; Berg-Sørensen, K.; Oddershede, L. B. *Chem. Rev.* **2017**, *117*, 4342−4375.

(5) Gawad, C.; Koh, W.; Quake, S. R. *Nat. Rev. Genet.* **2016**, *17*, 175−188.

(6) Rutledge, H.; Tezcan, F. *Chem. Rev.* **2020**, *120*, 5158−5193.

(7) Zheng, M. Q.; Kang, Y. F.; Liu, D.; Li, C. Y.; Zheng, B.; Tang, H. W. *Sens. Actuators B Chem.* **2020**, *319*, 128263.

(8) Nishiyama, K.; Mizukami, R.; Kuki, S.; Ishida, A.; Chida, J.; Kido, H.; Maeki, M.; Tani, H.; Tokeshi, M. *Biosens. Bioelectron.* **2022**, *198*, 113832.

(9) Gao, P.; Pan, W.; Li, N.; Tang, B. *Chem. Sci.* **2019**, *10*, 6035−6071.

(10) Zheng, G. L.; Zhao, L.; Yuan, D. Y.; Li, J.; Yang, G.; Song, D. X.; Mia, H.; Shu, L. J.; Mo, X. M.; Xu, X. D.; Li, L.; Song, X.; Zhao, Y. Y. *Biosens. Bioelectron.* **2022**, *198*, 113827.

(11) Lopez, A.; Liu, J. W. *Anal. Chem.* **2021**, *93*, 3018−3025.

(12) Wang, H. Y.; Ruan, Y. F.; Zhu, L. B.; Shi, X. M.; Zhao, W. W.; Chen, H. Y.; Xu, J. J. *Angew. Chem., Int. Ed.* **2021**, *60*, 13244−13250.

(13) He, X. L.; Ewing, A. *Angew. Chem., Int. Ed.* **2022**, *61*, e202116217.

(14) Wang, Y.; Gu, C. Y.; Ewing, A. *Angew. Chem., Int. Ed.* **2022**, *61* (20), e202200716.

(15) Marinesco, S. *Curr. Opin. Electrochem.* **2021**, *29*, 100746.

(16) Xiong, H. J.; Liu, L.; Wang, Y. H.; Jiang, H.; Wang, X. M. *Small.* **2022**, *18*, 2104341.

(17) Zhang, X. Y.; Song, C. X.; Yang, K.; Hong, W. W.; Lu, Y.; Yu, P.; Mao, L. Q. *Anal. Chem.* **2018**, *90*, 4968−4971.

(18) Zhao, N.; Coyne, J.; Xu, M.; Zhang, X.; Suzuki, A.; Shi, P.; Lai, J.; Fong, G. H.; Xiong, N.; Wang, Y. *Chem. Mater.* **2019**, *31*, 1006.

(19) Humenik, M.; Preiß, T.; Gödrich, S.; Papastavrou, G.; Scheibel, T. *Mater. Today Bio.* **2020**, *6*, 100045.

(20) Li, J.; Xun, K. Y.; Pei, K.; Liu, X. J.; Peng, X. Y.; Du, Y. L.; Qiu, L. P.; Tan, W. H. *J. Am. Chem. Soc.* **2019**, *141*, 18013−18020.

(21) Yue, Q. W.; Li, X. C.; Wu, F.; Ji, W. l.; Zhang, Y.; Yu, P.; Zhang, M. N.; Ma, W. J.; Wang, M.; Mao, L. Q. *Angew. Chem., Int. Ed.* **2020**, *59*, 11061−11065.

(22) Pan, C.; Wei, H.; Han, Z. J.; Wu, F.; Mao, L. Q. *Curr. Opin. Electrochem.* **2020**, *19*, 162−167.

(23) Zheng, J. Y.; Li, X. X.; Wang, K.; Song, J. J.; Qi, H. L. *Anal. Chem.* **2020**, *92*, 10940−10945.

(24) Geng, X.; Sun, Y. Q.; Guo, Y. F.; Zhao, Y. M.; Zhang, K.; Xiao, L. H.; Qu, L. B.; Li, Z. H. *Anal. Chem.* **2020**, *92*, 7940−7946.

(25) Han, X.; Wang, L.; Qi, B.; Yang, X.; Wang, E. *Anal. Chem.* **2003**, *75*, 6566−6570.

(26) Hou, H. F.; Jin, Y.; Wei, H.; Ji, W. L.; Xue, Y. F.; Hu, J. B.; Zhang, M. N.; Jiang, Y.; Mao, L. Q. *Angew. Chem., Int. Ed.* **2020**, *59*, 18996−19000.

(27) Liu, J. Y.; Dong, S. J. *Electrochem. Commun.* **2000**, *2*, 707−712.

(28) Deinhammer, R. S.; Ho, M.; Anderegg, J. W.; Porter, M. D. *Langmuir.* **1994**, *10*, 1306−1313.

(29) Nordberg, R.; Albridge, R. G.; Bergmark, T.; Ericson, U.; Hedman, J.; Nording, C.; Siegbahn, K.; Lindberg, B. *Nature* **1967**, *214*, 481−482.

(30) Arai, S.; Kriszt, R.; Harada, K.; Looi, L.; Matsuda, S.; Wongso, D.; Suo, S.; Ishiura, S.; Tseng, Y.; Raghunath, M.; Ito, T.; Tsuboi, T.; Kitaguchi, T. *Angew. Chem., Int. Ed.* **2018**, *57*, 10873−10878.

(31) Ino, K.; Nashimoto, Y.; Taira, N.; Azcon, J. R.; Shiku, H. *Electroanal.* **2018**, *30*, 2195−2209.

(32) Rojas, D.; Hernández-Rodríguez, J. F.; Pelle, F. D.; Escarpa, A.; Compagnone, D. *Microchim. Acta.* **2022**, *189*, 1−22.

(33) Xia, C.; Huang, W.; Kang, X.; Chen, P. Y.; You, L. J.; Guo, L. Q. *Microchim. Acta.* **2022**, *189*, 1−9.

(34) Fan, S. J.; Wang, X. Y.; Li, Y. L.; Chen, X. F.; Chen, H. T.; Schultz, Z. D.; Li, Z. *ACS Sens.* **2022**, *7*, 1431−1438.

(35) Gouridis, G.; Hetzert, B.; Kiosze-Becker, K.; Boer, M.; Heinemann, H.; Nürenberg-Goloub, E.; Cordes, T.; Tampé, R. *Cell Rep.* **2019**, *28*, 723−734.

(36) Imamura, H.; Huynh Nhat, K. P.; Togawa, H.; Noji, H. *Proc. Natl. Acad. Sci. U.S.A.* **2009**, *106*, 15651−15656.

(37) Özkan, A.; Atar, N.; Yola, M. L. *Biosens. Bioelectron.* **2019**, *130*, 293−298.

(38) Song, W. T.; Chen, Z.; Shi, C. Z.; Gao, Y. Y.; Feng, X. Y.; Li, H. W.; Li, Z. M.; Zhang, M. Z. *Blood.* **2021**, *138*, 3987.

(39) Ji, P. H.; Zhang, S. Y.; Liu, P. L.; Li, X.; Bao, W. C.; Cui, X. Z.; Huo, M. F.; Shi, J. L. *Nano Today.* **2022**, *44*, 101511.